

## Continuum and atomistic studies of a disclinated crack in a bicrystalline nanowire

K. Zhou,<sup>1</sup> A. A. Nazarov,<sup>2</sup> and M. S. Wu<sup>1,\*</sup>

<sup>1</sup>*Division of Engineering Mechanics, School of Mechanical and Aerospace Engineering, Nanyang Technological University, 50 Nanyang Avenue, 639798 Singapore*

<sup>2</sup>*Ufa State Aviation Technical University, 12 K. Marx Strasse, 450000 Ufa, Russia*

(Received 9 August 2005; revised manuscript received 11 October 2005; published 12 January 2006)

Intergranular crack formation in a cylindrical bicrystalline Ni nanowire containing a negative wedge disclination is studied via continuum mechanics and atomistic simulations. The continuum theory predicts a critical disclination strength above which the disclination is unstable and an equilibrium crack can grow from it. For the atomistic simulations, a disclination is inserted into an fcc cylinder of 25 nm radius containing a special  $\Sigma=5(310)$  ( $\theta=53.13^\circ$ ) tilt grain boundary. Molecular statics relaxations are then performed starting from structures both without and with an initial interfacial crack. The continuum and atomistic calculations show very close agreement in the critical disclination strength ( $11.6^\circ$  and  $11.1^\circ$ , respectively, for a nanowire of 25 nm radius), and general agreement in the stable crack length, the crack opening profile, and the stress field of the disclinated crack in the nanowire. Critical disclination strengths in the range of  $4^\circ$ – $6^\circ$  are also predicted for nanostructured materials prepared by severe plastic deformation for grain sizes in the range of 200–100 nm.

DOI: [10.1103/PhysRevB.73.045410](https://doi.org/10.1103/PhysRevB.73.045410)

PACS number(s): 61.72.Lk, 62.25.+g

### I. INTRODUCTION

In the last decades, ultrafine-grained (UFG) or nanostructured materials have been the subject of great scientific interest.<sup>1–6</sup> Experiments have shown that these materials can have significantly modified physical properties as compared to their coarse-grained counterparts<sup>1–4</sup> and a unique combination of mechanical properties such as high strength and high ductility.<sup>5,6</sup> To take full advantage of UFG materials, their fracture mechanisms and the basic factors influencing their strength should be addressed in detail. Recently, a few molecular dynamics simulations of the fracture behavior of nanocrystalline metals have been performed.<sup>7,8</sup> In these studies, however, only nanocrystals with the lowest grain sizes (12 nm and less) were considered and only the effect of the small grain size was addressed. Meanwhile, experiments and theoretical modeling show that UFG materials contain disclinations (rotational defects),<sup>9,10</sup> which induce high long-range stresses. These defects have different origins for nanocrystals prepared by different methods. In UFG metals produced by severe plastic deformation,<sup>2,5,6</sup> they form at triple grain boundary (GB) junctions due to an accumulation of dislocations at GBs caused by incompatibilities in the strain of grains.<sup>11–14</sup> In heavily deformed metals, junction disclinations with a strength up to  $3^\circ$  have been observed by transmission electron microscopy.<sup>11,15,16</sup> Disclinations inside grains were observed by high-resolution electron microscopy in mechanically milled, nanocrystalline iron.<sup>17</sup> In nanocrystals prepared by inert gas condensation followed by compaction disclinations can form both in nanoparticles during their growth and in GBs and junctions during the subsequent consolidation.<sup>18</sup> Disclinations can form also due to a termination of GBs during the growth of crystal thin films on substrates.<sup>19</sup>

Due to the singular internal stress fields induced by disclinations, they serve as preferential sites for crack formation.<sup>9,10,20</sup> Consequently, the investigation of the mechanisms of crack formation near disclinations and the

study of the crack characteristics are of fundamental importance for predicting the durability of nanostructured films, coatings, and bulk materials.

The first model of crack formation at a triple junction disclination was proposed by Rybin and Zhukovskii.<sup>20</sup> Assuming a cleavage energy of  $2 \text{ J m}^{-2}$ , for the grain size of  $0.5 \mu\text{m}$  they predicted that a wedge disclination with a strength of  $1.7^\circ$  had an equilibrium crack length of about  $0.07 \mu\text{m}$ . Essentially the same estimate was obtained by Gutkin and Ovid'ko for unsplit wedge disclinations.<sup>21</sup> These authors also predicted that the splitting of disclinations into ones with smaller strengths resulted in an amorphization of junctions and an increase of the equilibrium crack length.

Accurate estimates of the crack length due to disclinations were made by Wu and Zhou.<sup>22</sup> In the cited paper, the stress intensity factors and the opening displacement of a crack in a finite isotropic homogeneous cylinder containing a negative wedge disclination were calculated. The theory was exact in the sense that all boundary conditions were satisfied properly and the stress redistribution due to the crack growth was taken into account intrinsically in the governing equations. The theory predicted the existence of two equilibrium crack lengths at any value of the disclination strength. The shorter crack is unstable and has a length decreasing with an increase of the cylinder radius and disclination strength, while the longer one is stable and exhibits an opposite dependence on the radius and strength. However, the crack was assumed to be a Zener-type crack growing from the disclination in one direction only. Examination of the stress field of a wedge disclination in a cylinder and atomistic simulations carried out by the present authors suggest that a real crack is more likely to grow in both directions and this has not been taken into account in all the cited works. In addition, it is not clear *a priori* that the results obtained by continuum mechanical calculations are applicable for nanometer-sized solids.

The formation and growth of cracks have been extensively studied by atomistic computer simulations.<sup>23–32</sup> These simulations, by the use of either molecular statics or molecu-

lar dynamics methods, allow the elucidation of the crack tip processes (cleavage or dislocation emission) and the calculation of the equilibrium crack lengths. However, the role of disclinations in crack formation has never been addressed by atomistic simulations.

The present paper is devoted to the study of the formation of a double-ended crack from a wedge disclination in a cylindrical nanowire by means of both continuum mechanics theory and atomistic computer simulations. Atomistic simulations for a particular cylinder radius, equal to 25 nm here, are used to validate the predictions of continuum mechanics analysis. These predictions are then used to estimate the critical disclination strength, at which a crack is initiated near the disclination core, and the equilibrium crack length as functions of the disclination strength for any value of the cylinder radius. Interpreting the cylinder radius as the screening distance for the disclination elastic fields, conclusions for bulk nanostructured materials will then be extracted. A bicrystalline cylinder is considered for the atomistic study, but for the simplicity of the continuum calculations an isotropic cylinder is assumed.

## II. CONTINUUM MODEL

### A. Problem description and boundary conditions

Consider a negative wedge disclination centered in an isotropic homogeneous cylinder of radius  $R$ , as illustrated in Fig. 1(a). The disclination has the strength  $\omega$ , its line coincides with the cylinder axis, and the plane strain condition is assumed. Denote the shear modulus and the Poisson's ratio of the cylinder material by  $G$  and  $\nu$ , respectively. Rectangular coordinates  $(x, y)$  and polar coordinates  $(r, \theta)$  are defined on a circular cross section of the cylinder, both originating at the disclination line. A crack of length  $2l$  with the disclination at its center is assumed for convenience to lie along the  $x$  axis, although for the isotropic material assumption the crack can be along any radial direction. Two sets of boundary conditions need to be satisfied in this problem. One is that the outer surface of the cylinder is traction-free with the radial and shear stresses being zero at  $r=R$ , i.e.,

$$\sigma_{rr}(R, \theta) = 0, \quad \sigma_{r\theta}(R, \theta) = 0. \quad (1)$$

The other is that the crack surface is traction-free with the normal and shear stresses being zero at the crack location, i.e.,

$$\sigma_{yy}(x, 0) = 0, \quad \sigma_{xy}(x, 0) = 0, \quad (-l \leq x \leq l). \quad (2)$$

### B. Solutions by superposition

To obtain the solutions for the crack, e.g., its stress intensity factor (SIF), the crack in the original problem of Fig. 1(a) is modeled by an initially unknown distribution of infinitesimal edge dislocations in Fig. 1(b). The transformed problem in Fig. 1(b) is further decomposed into the two additive subproblems of Figs. 1(c) and 1(d), in which the cylinder is subjected to the internal loading of the disclination and that of the distribution of edge dislocations with unknown densities  $\rho_x$  and  $\rho_y$  (the subscripts  $x$  and  $y$  represent

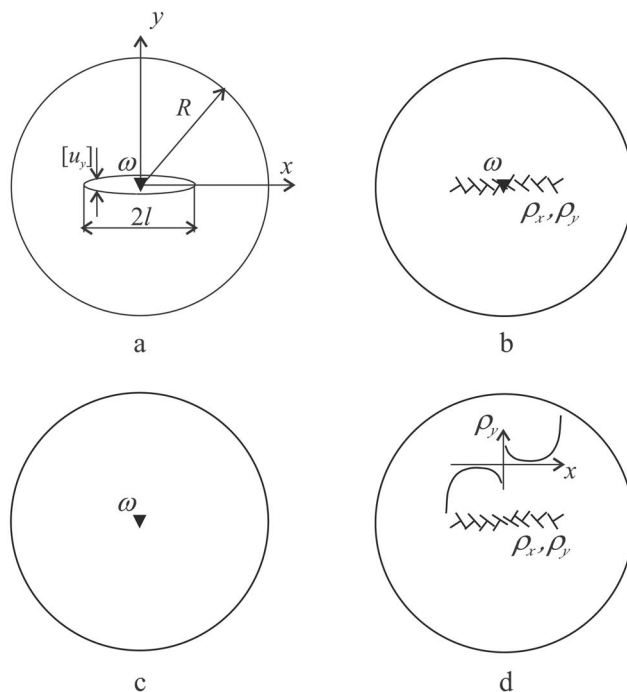


FIG. 1. Decomposition of the original problem into subproblems 1 and 2. (a) Original problem of a double-ended crack (length  $2l$ ) due to a negative disclination (strength  $\omega$ ) at the center of a cylinder (radius  $R$ ). (b) Modeling the crack by a distribution of edge dislocations with densities  $\rho_x$  and  $\rho_y$ . (c) Subproblem 1: the cylinder containing the disclination at its center. (d) Subproblem 2: the cylinder containing the distribution of edge dislocations at the original crack location.

two Burgers vector components of the edge dislocations), respectively. The fundamental solutions selected for each subproblem, i.e., the stress field of a disclination in a finite cylinder in subproblem 1 and that of an eccentrically located disclination in a finite cylinder in subproblem 2, automatically satisfy Eq. (1). In contrast, Eq. (2) is satisfied only after the superposition of the two subproblems, which leads to the solutions of  $\rho_x$  and  $\rho_y$ . Therefore the solution method is exact in the sense that all the boundary conditions are satisfied properly and any stress distribution due to crack growth is taken into account intrinsically. Stress redistribution is neglected in almost all previous works on disclinated cracks, i.e., the disclination stress field is assumed to be undisturbed by the crack.

In the subproblem of Fig. 1(c), the Airy stress function for a wedge disclination lying along the axis of a cylinder has been given by Romanov and Vladimirov as<sup>9</sup>

$$\chi^{\nabla} = \frac{1}{2} D \omega (x^2 + y^2) \left[ \ln \left( \frac{\sqrt{x^2 + y^2}}{R} \right) - \frac{1}{2} \right], \quad (3)$$

where  $D = G/2\pi(1-\nu)$ . The normal and shear stress components on the plane  $y=0$  due to the disclination are obtained by differentiating Eq. (3) and subsequently setting  $y=0$ , i.e.,  $\sigma_{yy}^{\nabla}(x, 0) = \partial^2 \chi^{\nabla} / \partial x^2|_{y=0}$  and  $\sigma_{xy}^{\nabla}(x, 0) = \partial^2 \chi^{\nabla} / \partial x \partial y|_{y=0}$ . The differentiation results show that the shear stress component is zero and the normal stress is symmetric about the origin,

which justifies the assumption of a double-ended crack of length  $2l$  wedged open by the disclination at the crack center.

In the subproblem of Fig. 1(d), the Airy stress functions for a discrete edge dislocation at the eccentric location  $(x,y)=(x',0)$  have been given by Eshelby as<sup>33</sup>

$$\begin{aligned} \chi_x^\perp &= Db_x(x') \left[ -y \ln\left(\frac{q_2}{q_1}\right) + \frac{R^2 y (R^2 - x'^2)}{q_1^2 x'^3} \left( x - \frac{R^2 + x'^2}{2x'} \right) \right], \\ \chi_y^\perp &= Db_y(x') \left[ (x-x') \ln\left(\frac{q_2 R}{q_1 x'}\right) + \frac{1}{2x'} (r^2 - R^2) (R^2 - x'^2) \right. \\ &\quad \left. \times \left( \frac{xx' - R^2}{q_1^2 x'^2} + \frac{1}{R^2} \right) \right], \end{aligned} \quad (4)$$

where  $b_x(x')$  and  $b_y(x')$  are the  $x$  and  $y$  components of the Burgers vector of the discrete dislocation, respectively, and  $r$ ,  $q_1$ , and  $q_2$  are given by  $r^2 = x^2 + y^2$ ,  $q_1^2 = (x - R^2/x')^2 + y^2$ , and  $q_2^2 = (x - x')^2 + y^2$ , respectively. The normal and shear stress components on  $y=0$  due to a discrete dislocation are then obtained as  $\sigma_{yy}^\perp(x,0;x') = \partial^2(\chi_x^\perp + \chi_y^\perp)/\partial x^2|_{y=0}$  and  $\sigma_{xy}^\perp(x,0;x') = \partial^2(\chi_x^\perp + \chi_y^\perp)/\partial x \partial y|_{y=0}$ . Note that  $b_y(x')$  and  $b_x(x')$  are present in  $\sigma_{yy}^\perp(x,0;x')$  and  $\sigma_{xy}^\perp(x,0;x')$ , respec-

tively, so that the expressions for the two stress components are decoupled. The stress components for a distribution of dislocations can be obtained by replacing  $b_x(x')$  and  $b_y(x')$  in  $\sigma_{xy}^\perp(x,0;x')$  and  $\sigma_{yy}^\perp(x,0;x')$  with  $\rho_x(x')dx'$  and  $\rho_y(x')dx'$ , respectively, and then taking integration with respect to  $x'$  from  $-l$  to  $l$ .

To satisfy Eq. (2), the normal and shear stresses at the crack location in the two subproblems are superimposed and set equal to zero, i.e.,

$$\sigma_{yy}^\nabla(x,0) + \int_{-l}^l \sigma_{yy}^\perp(x,0;x') dx' = 0, \quad (5)$$

$$\sigma_{xy}^\nabla(x,0) + \int_{-l}^l \sigma_{xy}^\perp(x,0;x') dx' = 0, \quad (6)$$

where  $-l \leq x \leq l$ . Equations (5) and (6) are two decoupled singular integral equations with the unknown density functions  $\rho_x(x')$  and  $\rho_y(x')$ , respectively. Since  $\sigma_{xy}^\nabla(x,0) = 0$ , it is easily determined that Eq. (6) has the solution  $\rho_x(x') = 0$ . This leaves only  $\rho_y(x')$  in Eq. (5) unsolved. Substituting the expressions for  $\sigma_{yy}^\nabla(x,0)$  and  $\sigma_{yy}^\perp(x,0;x')$  [with  $b_y(x')$  replaced by  $\rho_y(x')dx'$ ] into Eq. (5) yields

$$\begin{aligned} \int_0^l \frac{\rho_y(x')}{x' - x} dx' + \int_0^l \left( \frac{1}{x' + x} + \frac{3R^6 x + R^2 x^3 x'^2 - (R^2 + x^2)(3R^4 x' - 2R^2 x'^3 + x x'^4)}{R^2 (R^2 - x x')^3} \right. \\ \left. - \frac{3R^6 x + R^2 x^3 x'^2 - (R^2 + x^2)(-3R^4 x' + 2R^2 x'^3 + x x'^4)}{R^2 (R^2 + x x')^3} \right) \rho_y(x') dx' = \omega \left( 1 + \ln \frac{x}{R} \right) \quad (0 \leq x \leq l). \end{aligned} \quad (7)$$

The integration range  $[0, l]$  in Eq. (7) has been changed from  $[-l, l]$  in Eq. (5) because the symmetry of the crack about the origin implies that the dislocation distribution for modeling the crack is antisymmetric about the origin, i.e.,  $\rho_y(x') = -\rho_y(-x')$  [see Fig. 1(d)]. Equation (7) is a Cauchy singular integral equation, and its right side consists of a logarithmic singularity at  $x=0$ . It is expected that  $\rho_y(x')$  will have singularities at  $x'=0$  and  $l$  which correspond to the disclination location and the crack tip location, respectively. To solve this equation, the numerical method of Gerasoulis is used.<sup>34</sup> His method has also been successfully adapted to the solutions of similar singular integral equations.<sup>22,35-37</sup>

Once  $\rho_y(x')$  is known, the stress field in the nanowire containing the disclinated crack, i.e., that shown in Fig. 1(a), can be determined. For instance, the stress component  $\sigma_{yy}(x,y)$  is the sum of the corresponding components in the subproblems of Figs. 1(c) and 1(d):

$$\sigma_{yy}(x,y) = \sigma_{yy}^\nabla(x,y) + \int_{-l}^l \sigma_{yy}^\perp(x,y;x') dx', \quad (8)$$

where  $\sigma_{yy}^\nabla(x,y)$  and  $\sigma_{yy}^\perp(x,y;x')$  are determined from the second order derivatives of the Airy stress functions, as were

similarly done for the special cases of  $\sigma_{yy}^\nabla(x,0)$  and  $\sigma_{yy}^\perp(x,0;x')$ . The disclinated crack is a pure mode I crack (with normal opening) since  $\rho_x(x') = 0$  implies that the crack does not have a mode II (tangential) opening. The mode I SIF of the crack can be determined from the following equation as  $x$  approaches the crack tip from outside the crack, i.e.,  $K_I = \lim_{x \rightarrow l} [\sqrt{2\pi(x-l)} \sigma_{yy}(x,0)]$ , where  $\sigma_{yy}(x,0)$  is the total stress component obtained by superposition. With reference to the work by Wu and Zhou,<sup>22</sup> if the integration interval  $[-l, l]$  is normalized to  $[-1, 1]$  the limit is obtained as

$$K_I = D \left( \frac{\pi^3 l}{2} \right)^{1/2} \phi_y(1), \quad (9)$$

where  $\phi_y(1)$  is the value of the function  $\phi_y(t)$  evaluated at the crack tip  $t=1$ , and  $\phi_y(t)$  is related to the dislocation density according to  $\rho_y(t) = \phi_y(t)/\sqrt{1-t^2}$ ,  $-1 \leq t \leq 1$ . Furthermore, the opening displacement  $[u_y(x,0)] = u_y(x,0^+) - u_y(x,0^-)$  in the  $y$  direction [see Fig. 1(a)] of the mode I crack can be obtained directly from the dislocation density  $\rho_y(x')$ :

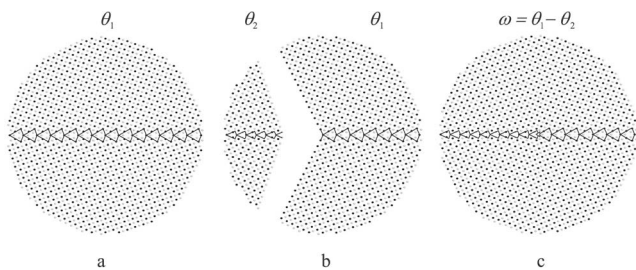


FIG. 2. Schematic of constructing an initial configuration in the atomistic model. (a) An fcc bicrystal with  $[001]$   $\theta_1=53.13^\circ$  tilt GB. (b) Two fcc bicrystals with  $[001]$   $\theta_2=36.87^\circ$  (left) and  $[001]$   $\theta_1=53.13^\circ$  (right) tilt GBs, respectively. (c) A bicrystalline nanowire containing an  $\omega=16.26^\circ$  wedge disclination, constructed from the two bicrystals in (b), along the central axis. Note that black and gray solid circles distinguish atoms lying on two successive  $(002)$  lattice planes.

$$[u_y(x,0)] = - \int_l^x \rho_y(x') dx' \quad (-l \leq x \leq l). \quad (10)$$

### III. ATOMISTIC MODEL

For the atomistic simulations, a disclination is inserted into a bicrystalline cylinder consisting of two fcc crystals with a common  $[001]$  axis initially delimited by a symmetric tilt GB with the reciprocal coincidence site density  $\Sigma=5$ , plane  $(310)$ , and misorientation angle  $\theta=53.13^\circ$  [Fig. 2(a)]. The tilt axis is parallel to the cylinder axis. In this case, the insertion of a disclination with strength  $\omega$  will delineate two  $[001]$  tilt GBs:  $\Sigma=5$   $\theta_1=53.13^\circ$  on one side and a boundary with misorientation angle  $\theta_2=\theta_1-\omega < \theta_1$  on the other side. To construct this system, two relaxed  $[001]$  bicrystals with misorientation angles  $\theta_1$  and  $\theta_2$  are prepared first by separate simulations using the same interatomic potential. These are cut along the  $\{110\}$  lattice planes as shown in Fig. 2(b) and the resulting wedges are brought into contact at a common origin. The  $\{110\}$  lattice planes of the two bicrystals will then be misoriented by the angle  $\omega/2=(\theta_1-\theta_2)/2$  and the lattices will overlap. To remove this overlap and match the lattice planes and thus finish the construction of the disclination, each atom of the system is displaced by a vector calculated on the basis of isotropic elasticity theory for wedge disclinations.<sup>38</sup> Eventually one obtains a disclinated cylinder shown in Fig. 2(c). Varying the misorientation angle  $\theta_2$  of the left bicrystal, one can vary the strength  $\omega$  of the disclination.

In the particular case presented in Fig. 2 the second GB is of the type  $\Sigma=5(210)$   $\theta_2=36.87^\circ$ , such that  $\omega=16.26^\circ$ . The GBs  $\Sigma=5(210)$  and  $(310)$  are two of the four favored GBs for the tilt axis  $[001]$ , each of which is composed of a contiguous sequence of one type of structural unit.<sup>39,40</sup> In Fig. 2 the structural units of these boundaries are outlined. The other two favored GBs for this axis are the crystal lattice planes  $(110)$  ( $\theta=0^\circ$ ) and  $(100)$  ( $\theta=90^\circ$ ). The structural units of the boundaries  $(110)$ ,  $(210)$ ,  $(310)$ , and  $(100)$  are denoted by the letters A, B, C, and D, respectively.<sup>41,42</sup> The atomic structures of all other GBs with this axis are described in the

structural unit model.<sup>39-41</sup> According to this model, each GB whose misorientation angle is intermediate between the misorientation angles of two adjacent favored GBs (e.g., B and C), consists of the structural units of these boundaries taken in a certain proportion and arrangement. The structural unit sequences per GB period characteristic of the GBs chosen to construct disclinations with varying strengths are presented in Table I. The dots in sequences characterizing the structure of centered GBs mean that the periods of these boundaries consist of two half-periods with the same stacking of units which are displaced with respect to each other by  $a_0/2$  along the tilt axis  $[001]$ .<sup>39</sup> The geometry of each GB in the table is characterized by two integers  $m$  and  $n$  the meaning of which is clear from Fig. 3, in which the left GB is a symmetric tilt boundary characterized by  $m=13$  and  $n=5$ . The period vector of the boundary can be represented through the crystallographic vectors of one of the grains as  $\vec{H}=m\vec{u}_1+n\vec{u}_2$ , where  $\vec{u}_1=(a_0/2)[1\bar{1}0]$  and  $\vec{u}_2=(a_0/2)[110]$  with  $a_0$  denoting the lattice parameter. The reciprocal coincidence site density of the boundary is calculated as  $\Sigma=(m^2+n^2)$  if  $m^2+n^2$  is odd, and  $\Sigma=(m^2+n^2)/2$  if  $m^2+n^2$  is even. In this case,  $\Sigma=97$ , and the misorientation angle is calculated as  $\theta=2 \arctan(n/m)=42.08^\circ$ . The right half-period of the boundary is represented in a nonrelaxed geometrical model, whereas the left one in the structural unit model. The structure described in the structural unit model is obtained from the geometrical one by combining each pair of atoms which are too close to each other near the GB plane into one atom (these pairs are enclosed by ellipses in Fig. 3) and subsequent atomic relaxation. In the structural unit model this GB is represented by the sequence BBBC.BBBC.

When bringing the two bicrystals into contact, one should bear in mind that in general they have different volume expansions. The volume expansion  $e$  of a GB is defined as the difference between the volumes of a bicrystal containing the boundary and an ideal crystal, both having the same number of atoms, per unit area of the boundary.<sup>40</sup> In terms of atomistic simulations,  $e$  is equal to a relative rigid-body shift of adjoining crystals in the direction normal to the GB plane during relaxation from an initial structure constructed by the use of the geometrical coincidence site lattice model. The difference of volume expansions will result in an edge dislocation with a Burgers vector normal to the GB plane that shares a line with the disclination. In order to study the effects caused purely by disclinations, the Burgers vector of this dislocation must be set to a minimum value. This can be done on the basis of the concept of geometrically necessary junction dislocations recently introduced for triple junctions.<sup>43</sup> This concept as applied to the junction of two boundaries under consideration is illustrated also in Fig. 3, which shows the construction of a disclination with the strength  $\omega=11.06^\circ$ . As the right half-period of the left GB is not decomposed into structural units, one can see that atoms on different  $\{110\}$  planes, two of which are marked by broken lines, are differently dislocated from the GB plane. The junction can be located at a line crossing an atom of any of the types denoted by the Greek letters  $\alpha$ ,  $\beta$ ,  $\xi$ , and  $\zeta$ . In Fig. 3 it will be located at a  $\zeta$ -type position. When welding the two bicrystals, atoms on the surface of the left bicrystal de-

TABLE I. Geometrical characteristics of the modeled GBs and disclinations.

Number	Structural unit sequence	$n/m$	$\theta$ (deg)	$\omega$ (deg)	$b$ (Å)
First GB					
C		1/2	53.13	0	N.A.
Second GB					
1	BBC	2/5	43.60	9.53	0.32
2	BBBCBBCBBCBBC. BBBCBBCBBCBBC	17/43	43.14	9.99	0.02
3	BBBCBBC. BBBCBBC	9/23	42.74	10.39	0.14
4	BBBC. BBBC	5/13	42.08	11.06	0.19
6	(3B)C(3B)C(4B)C	8/21	41.71	11.42	0.03
7	(3B)C(4B)C. (3B)C(4B)C	11/29	41.54	11.59	0.05
8	BBBBBC	3/8	41.11	12.02	0.10
9	(6B)C	4/11	39.97	13.16	0.01
10	(10B)C	6/17	38.88	14.25	0.04
11	B.B	1/3	36.87	16.26	0.55
12	A(10B)	5/16	34.71	18.42	-0.02
13	A(3B).A(3B)	3/11	30.51	22.61	-0.07

The letters A, B, and C denote the structural units of the GBs  $\Sigma=0/0^\circ$ ,  $\Sigma=5/36.87^\circ$ , and  $\Sigma=5/53.13^\circ$ , which are favored boundaries for the tilt axis [001] (Refs. 39 and 40).  $n$  and  $m$  are two integers determining the geometry of the boundaries; the misorientation angle is defined as  $\theta=2 \arctan(n/m)$ . Minimum possible value of the net dislocation Burgers vector is also presented.

pictured by open circles must be superposed with gray atoms of the right bicrystal and deleted (in fact, these circles illustrate empty sites). As one can see from the figure, this will involve not only a rotation corresponding to the disclination but also a translation normal to the GB plane to a distant  $\Delta b$  equal to the distance between the two closely spaced atoms on the edge of the left bicrystal. This translation forms a geometrically necessary dislocation whose Burgers vector magnitude  $\Delta b$  oscillates with the position of the junction. For a junction located at an  $\alpha$ -type position  $\Delta b=0$ . In addition, volume expansions of both bicrystals will occur during re-

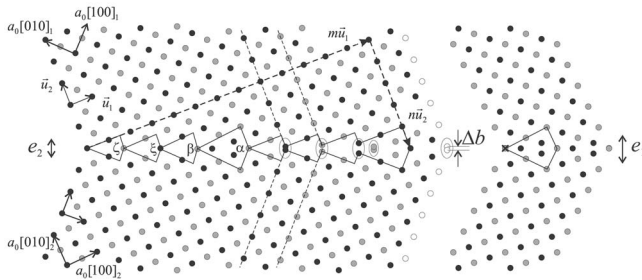


FIG. 3. Detailed schematic of the construction of a junction disclination from two bicrystals. The left GB is a  $\Sigma=97$  ( $\theta=42.08^\circ$ ) GB with parameters  $m=13$  and  $n=5$ . The left half-period of this GB is shown as decomposed into structural units (indicated by closed polygons) in the BBBC stacking, of which atoms  $\alpha$ ,  $\beta$ ,  $\xi$ , and  $\zeta$  occupy the possible positions for locating a disclination line. When two bicrystals are brought into contact to form the disclination, the open circles of the left bicrystal are replaced by the gray atoms of the right bicrystal. The junction line will coincide with the chain of gray atoms normal to the plane of view, as marked by the cross symbol.

laxation as indicated by double arrows in the figure. Therefore the net Burgers vector magnitude of the junction disclination will be equal to  $b=\Delta b+e_2-e_1$ . Varying  $\Delta b$  this Burgers vector can be made as close to zero as possible.

Table I summarizes the characteristics of GBs used to construct disclinations and the strength values of the resulting disclinations, which are used for simulations in the present paper. For convenience, the negative signs for the disclination strengths are dropped here and elsewhere. The minimum Burgers vector magnitudes of the accompanying disclinations are also presented in the table.

Disclinations constructed by the proposed method can be considered as junction disclinations, since they form a junction of two GBs having different misorientation angles. Elastically, they are equivalent to disclinations introduced either in a perfect crystal or in a tricrystal or any other aggregate provided that the properties of the crystals are isotropic. On the atomic level, they will be similar to triple junction disclinations. Therefore the results obtained in the present paper can be extended to predict some properties of triple junction disclinations.

In the simulations, disclinations are inserted into cylinders with an initial radius of  $R=25$  nm. The systems constructed contain about  $2.6 \times 10^5$  atoms. They serve as ready initial configurations for one series of the simulations, in which the behavior of growing cracks is studied. In the other series of simulations, initial cracks are inserted into the disclinated cylinder. The crack is opened by a simple construction of an approximate displacement field for atoms in the region  $|x| < l_0$ ,  $|y| < y_0 \approx l_0$  such that there are no too closely spaced atoms. This allows us to avoid instabilities at the start of simulations. For small values of the disclination strength smaller initial cracks are inserted and they have the shape of

a double-ended wedge of half-length  $l_0$ . For large values of the disclination strength long elliptic cracks are inserted with the long half-axis length  $l_0$ . In all cases  $l_0$  is chosen to be slightly larger than the crack half-length predicted by the continuum calculations for given values of  $\omega$ . These structures with initial cracks are designed to study the behavior of closing cracks.

Starting from the initial structures described above, the structures of disclinated cylinders are simulated by molecular statics, i.e., by energy relaxation at zero absolute temperature. Interatomic forces are described by the embedded atom method (EAM).<sup>44</sup> A potential of this method for Ni is used. It is fitted to the lattice period  $a_0=3.52 \text{ \AA}$ , and the elastic constants  $c_{11}=233 \text{ GPa}$ ,  $c_{12}=154 \text{ GPa}$ , and  $c_{44}=128 \text{ GPa}$ . The cutoff distance of the original potential is equal to  $r_c=4.8 \text{ \AA}$ . The above values of the elastic constants are also used to calculate Voigt averages for the shear modulus and Poisson ratio:  $G=92.6 \text{ GPa}$  and  $\nu=0.281$ . These values are used to calculate the crack characteristics in the continuum mechanics approach.

Relaxation is performed by the code XMD—Molecular Dynamics for Metals and Ceramics authored by J. Rifkin at the University of Connecticut.<sup>45</sup> This method adds some distance to the cutoff distance  $r_c$ , so that  $r_c=5.8 \text{ \AA}$ . Due to this, the minimum simulation cell size along the  $[001]$  direction compatible with the minimum image convention<sup>46</sup> is equal to  $H_z=4a_0=14.08 \text{ \AA} > 2r_c$ . Fixed periodic boundary conditions are applied in this direction, since we consider the disclination under the plane-strain condition. In the other two directions the system has finite sizes, i.e., the cylinder has a free lateral surface.

For an estimate of the critical SIF  $K_{IC}=\sqrt{4\gamma_f G/(1-\nu)}$  the cleavage energy  $2\gamma_f$  should be known. This parameter is calculated in the atomistic model for two GBs, the right boundary  $\Sigma=5(310)$  and a sample left boundary  $\Sigma=5(210)$  (GB No. 11 in Table I), as a difference between the energies of a bicrystal with separated grains and the one having a relaxed GB structure:  $2\gamma_f=2\gamma_s-\gamma$ , where  $\gamma_s$  and  $\gamma$  are the specific surface and GB energies. For both boundaries the value of  $2\gamma_f=2.22 \text{ J m}^{-2}$  has been found. This value is used for the estimate of the critical SIF:  $K_{IC}=0.756 \text{ MPa m}^{1/2}$  in the continuum model that assumes a symmetric crack. In general, other GBs listed in Table I can have cleavage energies different from this value and this can result in some fine effects on the crack formation as will be discussed below. However, the differences are not too large, as can be deduced, for example, from the maximum difference of about  $0.2 \text{ J m}^{-2}$  between the energies of  $[001]$  GBs in Ni in the misorientation interval  $36.87^\circ\text{--}53.13^\circ$ .<sup>42</sup>

#### IV. RESULTS

##### A. Numerical estimates by continuum model

The SIFs are calculated for a disclinated crack in a bicrystalline cylinder with  $R=25 \text{ nm}$ . Figure 4 plots the dependence of the SIF on the normalized half-crack length  $l/R$  for some of the values of  $\omega$  shown in Table I.

Analyzing Fig. 4 one can come to the following conclusions. For  $\omega < 11.56^\circ$ , the SIFs are less than the critical SIF

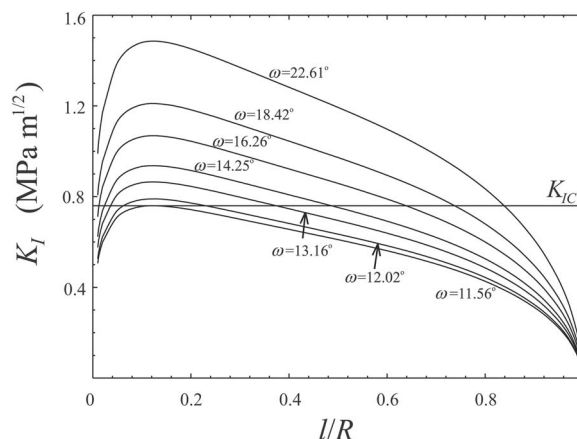


FIG. 4. Variation of the model I SIF with the normalized half-crack length  $l/R$  for different disclination strengths  $\omega$ . The nanowire radius is  $R=25 \text{ nm}$ . The critical disclination strength for crack formation is  $\omega=11.56^\circ$ , estimated from the curve tangential to the straight line  $K_{IC}=0.756 \text{ MPa m}^{1/2}$ . For  $\omega > 11.56^\circ$ , the  $K_{IC}$  line intersects the curves at two locations, which correspond to two equilibrium crack lengths.

for all crack lengths. This means that below the value  $\omega_c \approx 11.6^\circ$ , referred to as the critical disclination strength, no crack can exist in the cylinder of the given radius. When  $\omega > \omega_c$  there are two values of the equilibrium crack length. The shorter crack is unstable, while the longer crack is stable. With increasing disclination strength the unstable crack length decreases, while the stable crack length increases.

The critical disclination strength is a physical characteristic, which is important for the failure prediction of materials containing disclinations. This characteristic depends on the screening radius of the long-range stresses of the defect (in this case, the radius of the cylinder). This dependence is illustrated in Fig. 5, which shows a linear relationship in log-log scale with a slope of  $-0.5$ . It can be interpolated with good accuracy by the relationship

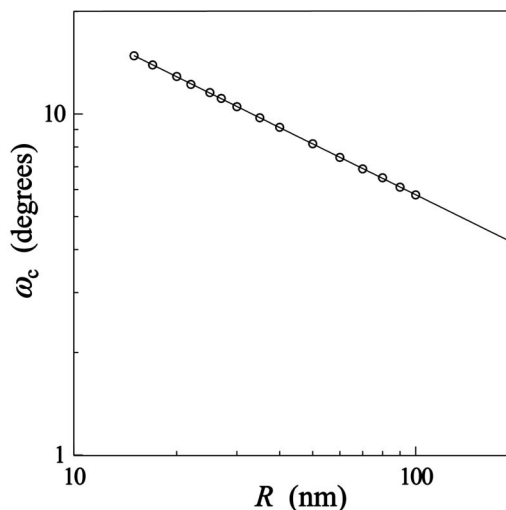


FIG. 5. Dependence of the critical disclination strength for crack formation on the nanowire radius.

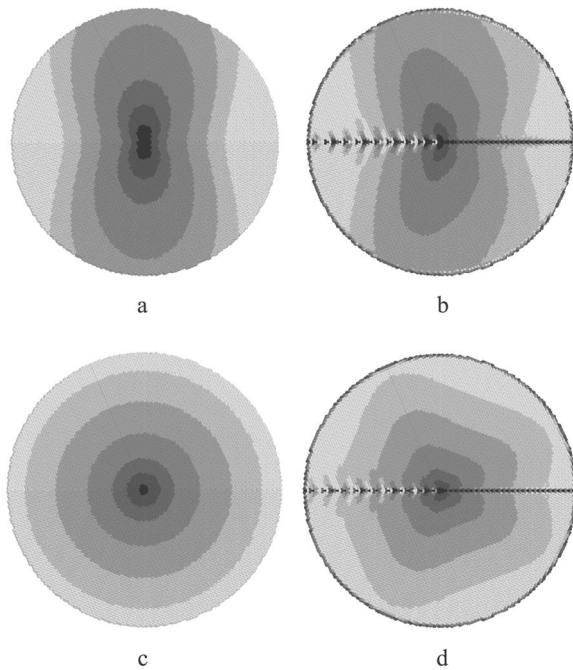


FIG. 6. Normal stress  $\sigma_{yy}$  maps (a, b) and hydrostatic stress  $\Sigma_{i=1}^3 \sigma_{ii}(x, y)/3$  maps (c, d) of a nanowire containing an  $11.06^\circ$  wedge disclination and a  $0.19 \text{ \AA}$  edge dislocation. The results in (a) and (c) are calculated by the continuum model, while those in (b) and (d) by the atomistic model. The nanowire has a radius of 25 nm, but the maps only represent the inner part of the nanowire with a radius of 15 nm. Stress contours from outer to inner part of cylinder: 0, 1, 2.5, 5, 7, and 10 GPa.

$$\log \omega_c = \log 55.7 - 0.5 \log R \quad \text{or} \quad \omega_c \approx \frac{55.7}{\sqrt{R}}, \quad (11)$$

where  $R$  is substituted in nm and  $\omega_c$  is in degrees. As one can see from this relationship, the critical strength of disclination slowly decreases with the increasing radius of the cylinder.

### B. Results of atomistic simulations

The simulations show that small-strength disclinations have a stable structure with a nonbroken core, which does not differ significantly from the initial structure. To compare the atomistic model with an elastic model of the disclination, maps of the normal stress  $\sigma_{yy}(x, y)$  and hydrostatic pressure  $\Sigma_{i=1}^3 \sigma_{ii}(x, y)/3$  are calculated using both methods for a disclination with the strength  $\omega = 11.06^\circ$  accompanied by a  $0.19 \text{ \AA}$  edge dislocation [Figs. 6(a)–6(d)]. In the atomistic model, the product of the stress at a given atomic site with the local atomic volume at this site is calculated.<sup>47</sup> The stress is then determined from this product by simply dividing it by the atomic volume of the ideal Ni lattice,  $V_a = 10.94 \text{ \AA}^3$ . Thus atomic level stresses are calculated approximately. Comparing the stress maps, one can make two important conclusions. First, there is a significant influence of the anisotropy on the stress distribution. Second, stress values in the far-field compare well, but near the disclination line stresses in the atomistic model increase more slowly than those in the elastic one.

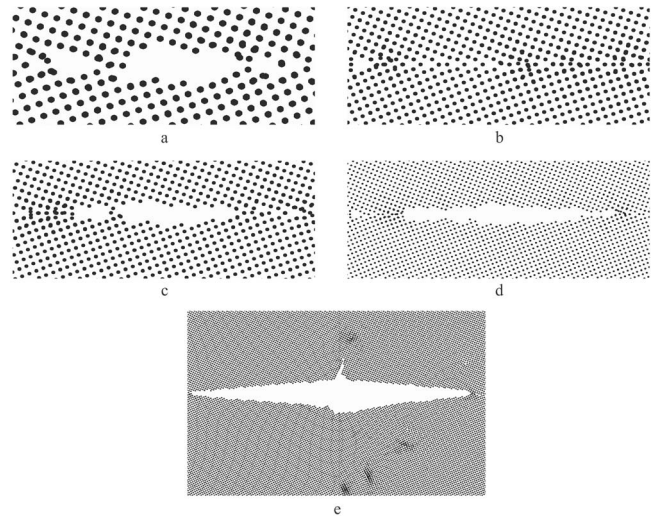


FIG. 7. Atomic structures near a negative wedge disclination with the strength equal to (a)  $9.99^\circ$ , (b)  $10.39^\circ$ , (c)  $11.06^\circ$ , (d)  $13.16^\circ$ , and (e)  $22.61^\circ$  obtained by relaxation from initial structures containing no cracks. Atoms on all (002) planes are represented by black circles. The studied nanowire has a radius of 25 nm and its center coincides with the center of each figure.

When the strength of the disclination increases, a greater disorder is observed in its core. At a certain value of the strength the disclination is no longer stable: it opens a crack along the GBs on both of its sides. With a further increase of the disclination strength the length of the crack also increases. Figure 7 shows the sequence of relaxed structures obtained with a crack-free initial structure. The critical disclination strength  $\omega_c$ , at which the disclination initiates a crack, cannot be exactly determined from the atomistic computations. For  $\omega = 9.99^\circ$  one sees a very small crack, while for  $\omega = 10.39^\circ$  no definite crack is observed, and at  $\omega = 11.06^\circ$  a crack is open again. This nonmonotonic behavior is most probably due to an interplay between the disclination strain energy release and the GB cleavage energy. The latter depends on the GB period. Generally, a shorter period GB has a lower energy and correspondingly higher cleavage energy. The left GB corresponding to  $\omega = 9.99^\circ$  has a longer period than that corresponding to  $\omega = 10.39^\circ$  and hence a smaller GB cleavage energy [compare GB periods  $h = a_0 \sqrt{(n^2 + m^2)}/2$  and the stacking of structural units for boundaries No. 2 and No. 3 in Table I]. At  $\omega > 11.06^\circ$  there are no stable disclinations: cracks will always nucleate. Consequently, the approximate value for the critical disclination strength at  $R = 25 \text{ nm}$  obtained from the above data is  $\omega_c \approx 11.1^\circ$ .

The cracks illustrated in Fig. 7 correspond to the stable cracks studied in Sec. II. In qualitative agreement with the results of the continuum model, the equilibrium length of these cracks increases with the strength of the disclination. However, the crack sizes determined from the atomistic simulations are nearly twice less than those predicted by the continuum approach for the same strength values (Fig. 4). Analysis of the atomic structures near cracks shows that the cracks do not open in a purely brittle matter. At disclination strengths close to  $\omega_c$  there is significant atomic disorder near

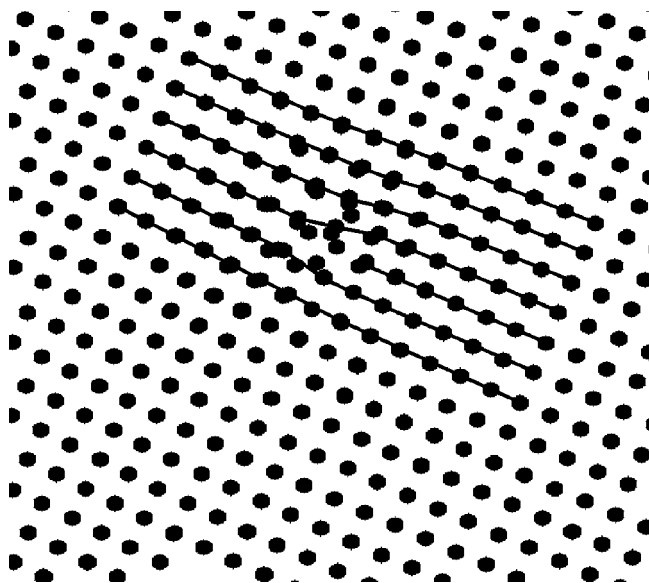


FIG. 8. Magnified view of Fig. 7(e), showing the emission of a dislocation from a disclinated crack during atomistic simulations.

the crack tips [Figs. 7(a)–7(c)]. At larger values of the disclination strength one observes the nucleation of a small crack ahead of the main crack [see the left side of Fig. 7(d)]. Such a behavior has been observed earlier by Farkas in the simulations of crack propagation under load in a NiAl ordered alloy.<sup>32</sup> At even larger disclination strength there is a significant relaxation of the disclination stress field by the emission of dislocations from the crack. For example, these dislocations are seen as black spots in Fig. 7(e) where a crack grown from the  $\omega=22.61^\circ$  disclination is illustrated. The dislocation seen on the upper part of Fig. 7(e) is visualized via a magnified view shown in Fig. 8. A further analysis shows that the dislocation has the Burgers vector  $\vec{b}=(a_0/2)[10\bar{1}]$ , which has a projection equal to  $a_0/2$  on the (001) plane. Corresponding (100) extra half-planes are easily detected in the figure for each dislocation.

**C. Comparison of continuum and atomistic model results**

In general, all cracks have the shape of a double-ended wedge as predicted by the continuum analysis. However, in many cases the cracks predicted by the atomistic method have asymmetric shapes: it usually propagates a longer distance along one of the GBs than along the other. In all these cases dislocation emission is observed mainly in the direction of the short wing of the crack. This indicates a significant trapping effect of the dislocation emission on the crack growth.

In order to exclude the dislocation emission, simulations with a starting structure containing an initial crack are also carried out for the same values of the disclination strength as described in Sec. III. In this case the tips of equilibrium cracks always have an ordered atomic structure. The results of these simulations are presented in Fig. 9, along with the data of continuum mechanics calculations. In this case a crack open near a disclination with the strength  $\omega=11.06^\circ$  is

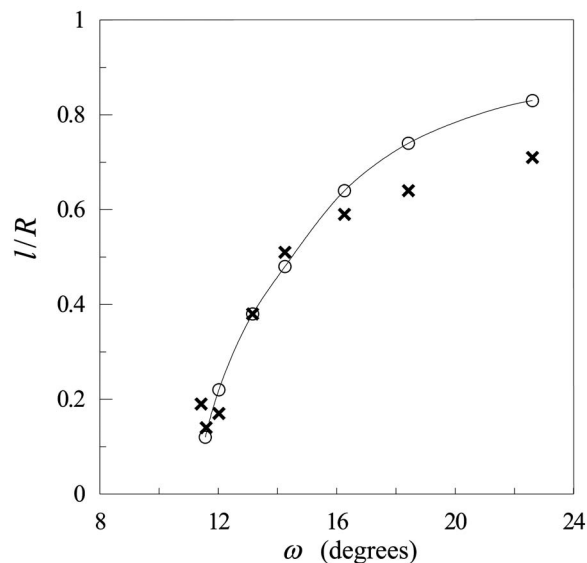


FIG. 9. Dependence of the stable crack length on the disclination strength as calculated by the continuum model (open circles) and the atomistic model (crosses). The studied nanowire has a radius of 25 nm.

closed back. At higher values of  $\omega$  the cracks are not closed. This confirms that the critical disclination strength is  $\omega_c \approx 11.1^\circ$ . As one can see from Fig. 9, stable crack lengths calculated by the atomistic simulations are now very similar to the values obtained from the continuum model calculations. At  $\omega$  slightly larger than  $\omega_c$ , there is a significant scatter of the values of the crack length calculated by the atomistic simulations around the continuum model predictions. At larger  $\omega$  the crack length increases monotonically. At  $\omega=13.16^\circ$  the agreement between the two calculations is very close, while at  $\omega=16.26^\circ$  the atomistic model result is approximately 15% less than the continuum model result. The discrepancy increases at large  $\omega$  when  $l \rightarrow R$ .

Figure 10 plots the distribution of the normal stress  $\sigma_{yy}$  around the disclinated crack of half-length  $l=0.38R$  in a nanowire of radius  $R=25$  nm. The disclination strength is  $\omega=13.16^\circ$ . The left and right parts of the figure show the predictions of the continuum and atomistic models, respec-

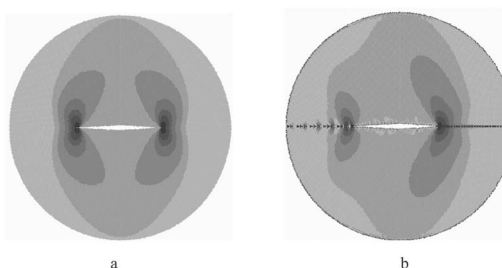


FIG. 10. Comparison of the maps of the normal stress  $\sigma_{yy}$ , which are calculated from the continuum model (a), and the atomistic model (b), respectively, in a nanowire of radius  $R=25$  nm containing a disclination of strength  $\omega=13.16^\circ$ . The nucleated crack due to the disclination reaches a half length of  $l=0.38R$  in both models. Stress contours from outer to inner part of cylinder: 0, 1, 2.5, 4, 5.5, and 9 GPa.

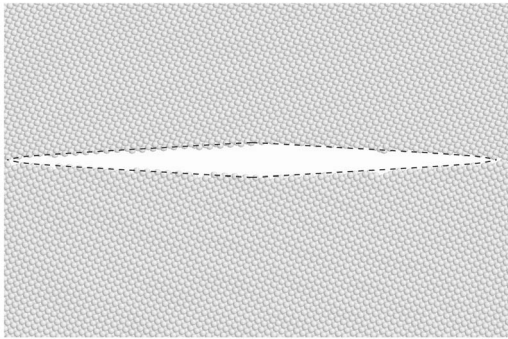


FIG. 11. Overlay of the crack profile (dotted line) predicted by the continuum model onto that predicted by the atomistic model for the same case presented in Fig. 10. The largest crack opening displacement is about 1.34 nm.

tively. It can be seen that the overall agreement is satisfactory, given the fact that the continuum model assumes isotropic homogeneous medium while the atomistic model does not. Dependences of the stress on distance from the crack tips and the stress concentrations near the tips as predicted by the two models are also very similar.

Figure 11 overlays the crack profile predicted by Eq. (10) onto that predicted by the atomistic simulation (with a starter crack) for the case of  $\omega = 13.16^\circ$  and  $R = 25$  nm. A very good agreement between the predictions of the two approaches is found. The largest crack opening displacement is estimated to be about 1.34 nm, and the half-crack length is  $l = 0.38R$ . Some disagreement, barely noticeable, arises from the slight asymmetry of the crack predicted by the atomistic model.

## V. DISCUSSION

In the continuum fracture mechanics approach, the stability of a preexisting crack under the given conditions is a key characteristic to be investigated. For instance, at  $K_I = K_{IC}$  a Griffith crack in an infinite medium subjected to a remote load normal to the crack is unstable, while it is stable if subjected to a normal line load acting at the crack surface. In a disclinated cylinder, Wu and Zhou were the first to show that there are two equilibrium crack lengths, one for an unstable crack and the second for a stable longer crack.<sup>22</sup> The unstable crack length was shown to decrease with an increase of the radius of the cylinder, i.e., the screening distance of the disclination long-range stresses, while the stable crack length depends on the cylinder radius in the opposite manner.

A new result of the present work, fundamentally different from the earlier studies of disclinated cracks, is that there exists a critical disclination strength  $\omega_c$  below which the disclination is stable with no crack formation while above which a crack can nucleate. This is predicted directly for the first time via atomistic simulations, and supported by the continuum model, which predicts that the critical  $K_I = K_{IC}$  condition can never be reached for any crack length for  $\omega < \omega_c$ , see Fig. 4. This introduces a new concept of critical disclination strength in the theory of fracture related to disclinations. The concept is important in that it determines the

influence of disclinations on the strength of materials. As shown by the present comparison, continuum mechanics calculations can predict this characteristic with good accuracy even for screening distances for the disclination stress field lying on the nanometer scale ( $\omega_c \approx 11.1^\circ$  vs  $11.6^\circ$  by atomistic calculation for  $R = 25$  nm). In addition to our recent results on the applications of the disclination-structural unit model to the calculations of GB energies,<sup>48–50</sup> the current work demonstrates that continuum mechanics models can have a good predictive capability on the nanoscale.

For  $\omega \geq \omega_c$ , the continuum model predicts unstable cracks less than a few nanometers in length. These predictions may be considered unphysical, and inaccurate at best, since the continuum theory is based on the linear elastic assumption without taking the disclination core structure into consideration. In the atomistic simulations starting from initial structures, which are nonequilibrium in nature since their displacement fields are given by linear elastic isotropic theory, the high internal strain within the disclination core would likely initiate a crack that extends unstably until it reaches its longer stable length. Any shorter unstable crack, even if it physically exists, will not be easily captured by the atomistic simulations due to the possibly unstable nature (as suggested by the continuum theory) and the nonequilibrium initial structures. Indeed, our atomistic simulations can only capture the stable cracks, also predicted by the continuum theory. From the current continuum and atomistic investigations, we cannot yet make definite conclusions on the existence of the nanometer-size unstable cracks.

Stable crack length above  $\omega_c$  has been shown to increase with the disclination strength by both approaches. However, there are discrepancies between the results of continuum mechanics predictions and atomistic simulations. They are particularly large for the first method of simulation starting from structures without an initial crack. These discrepancies warrant several explanations.

First, continuum mechanics calculations are performed in the isotropic theory of linear elasticity. The significance of elastic anisotropy is demonstrated in Fig. 6, which shows the different shapes of the stress field calculated via the isotropic theory and via the atomistic theory that is essentially anisotropic. However, the errors due to this factor are not expected to be too large in certain situations. For example, recent studies of brittle fracture in iron have shown that critical loadings for cleavage calculated for different crack orientations from anisotropic theory differ by no more than 10% from each other.<sup>31</sup> Therefore an error of the order of 10% may also be expected when calculating this parameter using isotropic theory. Nevertheless, as one can see from Fig. 4, a small error of 10% in estimating the critical SIF can significantly change the equilibrium crack length prediction.

Second, fracture is not purely brittle in the atomistic simulations. In the first method of simulation, the crack tip regions have a disordered atomic structure even when  $\omega$  is slightly above  $\omega_c$  [Figs. 7(a)–7(c)]. A part of the disclination strain energy is spent on this disordering and the crack stops at a length smaller than that predicted for ideal brittle fracture. At higher disclination strength values this disorder is retained. Moreover, some additional features appear. In some cases, a small crack can nucleate ahead of the main crack and

separate from it by an uncleaved region [Fig. 7(d)]. At even larger strength, a significant part of the disclination strain energy is spent via another channel of relaxation: dislocation emission [Fig. 7(e)]. This phenomenon is very common for fracture in metals.<sup>29,30</sup> Furthermore, even if a brittle fracture can occur in real Ni bicrystals at certain given conditions, empirical potentials may not make such a prediction. Recent studies of crack propagation in silicon, for example, have shown that most of the empirical potentials predict ductile fracture, often in contradiction with experiments indicating brittle fracture.<sup>24</sup>

The third factor that can significantly influence the equilibrium crack length prediction is lattice trapping, which is caused by the periodicity of the lattice. A crack in the lattice overcomes a periodic energy barrier that can arrest its motion. This is similar to the trapping of lattice dislocations by the Peierls barrier. It is well-known that due to the lattice trapping a crack can be stable and cannot advance up to a load  $K_I^+ > K_{IC}$ , or can be stable and cannot heal down to a load  $K_I^- < K_{IC}$ .<sup>25</sup> Therefore, for a real crack in the discrete lattice there may be a dead zone corresponding to a certain interval with boundaries below and above the equilibrium length predicted by the continuum theory.

The agreements between the predictions of the two approaches are much better, however, when the atomistic simulations are carried out using the second method, i.e., by introducing an initial crack. At intermediate values of the disclination strength  $\omega = 14^\circ - 16^\circ$  the difference in predictions is about 15%. At  $\omega$  slightly above the critical value there is some scatter of the simulation results around the continuum predictions. In this region, most probably, the discreteness of the structure of the left GB, which changes non-monotonically with the misorientation angle, plays an important role. At high  $\omega$  the cracks have a length comparable to the cylinder diameter. In the atomistic model, there is a significant surface tension that is not taken into account in the mechanics model. This surface tension induces a bulk compression, which is nonuniform due to crack perturbation, that might have a larger influence on the length of longer cracks than on that of shorter ones. This is because a longer crack, being closer to the cylinder boundary, interacts strongly with the surface tension and also redistributes the stress significantly compared to a shorter crack. This can explain the increase of discrepancies between the results at large disclination strengths.

It is also noteworthy that the atomistic and continuum approaches yield reasonably consistent predictions in the crack opening displacement and the stress distribution in the nanowire containing the disclinated crack. This is in spite of the fact that the nanowire is not only elastically anisotropic but also bicrystalline in the atomistic model, while it is purely isotropic and monocrystalline in the continuum model. Continuum solutions for a finite anisotropic and inhomogeneous medium containing a wedge disclination or even an edge dislocation, are not presently available.

In view of the above discussion, the consistency between the results of atomistic simulations and continuum mechanics calculations can be considered quite satisfactory in terms of the predictions of the critical disclination strength, the stable crack length, the crack opening displacement, and the stress field in the nanowire.

The obtained results can be used to estimate the critical strength of disclinations in nanostructured metals. The stress fields of a single disclination in a cylinder are screened on a distance equal to the cylinder radius  $R$ .<sup>9,10</sup> In a polycrystal, the screening distance for the stress fields is of the order of the grain size  $d$ . Therefore the cylinder radius  $R$  in this case should be replaced by the grain size  $d$ :  $R \approx d$ . Then, by Eq. (11)  $\omega_c \approx 5.6^\circ$  for  $d = 100$  nm and  $\omega_c = 3.9^\circ$  for  $d = 200$  nm. These estimates are applicable to UFG metals prepared by severe plastic deformation.<sup>2,4</sup> However, disclinations in polycrystals are coupled into dipoles and quadrupoles.<sup>11,13</sup> Taking such  $n$ -pole configurations into account, the estimated critical strength may further decrease. With this note, the above estimates seem not inconsistent with the results of experimental measurements, which show the existence of disclinations with strengths up to  $3^\circ$  in triple grain junctions of heavily deformed metals.<sup>15,16</sup> Further research on the critical behavior of disclinations in multipole configurations is necessary to shed light on this issue.

## VI. CONCLUSIONS

In this paper, the atomistic and continuum models are used for the first time to investigate a double-ended disclinated crack in a cylindrical nanowire of nickel. The continuum model for fracture takes into account the stress redistribution due to crack generation in a finite isotropic cylinder. The atomistic model is based on constructing a certain initial structure for the wedge disclination in a bicrystalline cylinder, which may or may not contain an initial crack, and the subsequent relaxation via molecular statics.

For a cylinder radius of 25 nm, the results of both the atomistic and continuum models show general agreement in the predicted critical disclination strength, the stable crack length, the crack opening profile, and the stress distribution in the cylinder. The key physical results are (1) the existence of a critical value ( $11.1^\circ - 11.6^\circ$  for the cylinder radius of 25 nm) for the disclination strength below which a crack cannot nucleate, (2) the decrease of the critical disclination strength with the inverse square root of the cylinder radius, and (3) the increase of the stable equilibrium crack length with the disclination strength. These results highlight certain fundamental characteristics of disclinated solids with implications on the reliability of nanostructured materials. As an important particular result, the limiting strength of disclinations in nanostructured metals as a function of the grain size can be estimated on the basis of the above results.

## ACKNOWLEDGMENTS

The authors would like to acknowledge the support of the Agency for Science, Technology and Research, Singapore (Grant No. 032 101 0019) in this investigation. A.A. Nazarov also acknowledges partial support of this research by the Russian Science Support Foundation and INTAS (Project No. 03-51-3779).

- \*Corresponding author. Email address: mmswu@ntu.edu.sg
- <sup>1</sup>H. Gleiter, *Prog. Mater. Sci.* **33**, 223 (1989).
  - <sup>2</sup>R. Z. Valiev, R. K. Islamgaliev, and I. V. Alexandrov, *Prog. Mater. Sci.* **45**, 103 (2000).
  - <sup>3</sup>*Nanostructured Materials*, edited by C. Koch (Noyes, Norwich, NY, 2002).
  - <sup>4</sup>A. A. Nazarov, and R. R. Mulyukov, in *Handbook of Nanoscience, Engineering, and Technology*, edited by W. A. Goddard, D. W. Brenner, S. Lyshevski, and G. Iafrate (CRC Press, Boca Raton, 2002), p. 22-1.
  - <sup>5</sup>R. Z. Valiev, *Nature (London)* **419**, 887 (2002).
  - <sup>6</sup>R. Z. Valiev, I. V. Alexandrov, Y. T. Zhu, and T. C. Lowe, *J. Mater. Res.* **17**, 5 (2002).
  - <sup>7</sup>D. Farkas, H. Van Swygenhoven, and P. M. Derlet, *Phys. Rev. B* **66**, 060101(R) (2002).
  - <sup>8</sup>A. Latapie and D. Farkas, *Phys. Rev. B* **69**, 134110 (2004).
  - <sup>9</sup>A. E. Romanov and V. I. Vladimirov, in *Dislocations in Solids*, edited by F. R. N. Nabarro (North-Holland, Amsterdam, 1992), Vol. 9, p. 191.
  - <sup>10</sup>A. E. Romanov, *Eur. J. Mech. A/Solids* **22**, 727 (2003).
  - <sup>11</sup>V. V. Rybin, *Large Plastic Deformations and Fracture of Metals* (Metallurgy, Moscow, 1986) (in Russian).
  - <sup>12</sup>V. V. Rybin, A. A. Zisman, and N. Yu. Zolotarevsky, *Sov. Phys. Solid State* **27**, 105 (1985).
  - <sup>13</sup>V. V. Rybin, A. A. Zisman, and N. Yu. Zolotarevsky, *Acta Metall. Mater.* **41**, 2211 (1993).
  - <sup>14</sup>A. A. Nazarov, A. E. Romanov, and R. Z. Valiev, *Acta Metall. Mater.* **41**, 1033 (1993).
  - <sup>15</sup>V. Klemm, P. Klimanek, and M. Motylenko, *Mater. Sci. Eng., A* **324**, 174 (2002).
  - <sup>16</sup>M. Motylenko, V. Klemm, P. Klimanek, T. Pavlovitch, and H. Straube, *J. Alloys Compd.* **378**, 93 (2004).
  - <sup>17</sup>M. Murayama, J. M. Howe, H. Hidaka, and S. Takaki, *Science* **295**, 2433 (2002).
  - <sup>18</sup>V. G. Gryaznov and L. I. Trusov, *Prog. Mater. Sci.* **37**, 289 (1993).
  - <sup>19</sup>X. Jiang and C. L. Jia, *Appl. Phys. Lett.* **69**, 3902 (1996).
  - <sup>20</sup>V. V. Rybin and I. M. Zhukovskii, *Sov. Phys. Solid State* **20**, 1056 (1978).
  - <sup>21</sup>M. Yu Gutkin and I. A. Ovid'ko, *Philos. Mag. A* **70**, 561 (1994).
  - <sup>22</sup>M. S. Wu and H. Zhou, *Int. J. Fract.* **82**, 381 (1996).
  - <sup>23</sup>R. L. B. Selinger and D. Farkas, *MRS Bull.* **25**, 11 (2000); P. Gumbsch and R. M. Cannon, *ibid.* **25**, 15 (2000).
  - <sup>24</sup>N. Bernstein and D. W. Hess, *Phys. Rev. Lett.* **91**, 025501 (2003).
  - <sup>25</sup>R. Pérez and P. Gumbsch, *Phys. Rev. Lett.* **84**, 5347 (2000).
  - <sup>26</sup>D. Holland and M. Marder, *Phys. Rev. Lett.* **80**, 746 (1998); *Adv. Mater. (Weinheim, Ger.)* **11**, 793 (1999).
  - <sup>27</sup>S. J. Zhou, D. M. Beazley, P. S. Lomdahl, and B. L. Holian, *Phys. Rev. Lett.* **78**, 479 (1997).
  - <sup>28</sup>J. Schiøtz and A. E. Carlsson, *Philos. Mag. A* **80**, 69 (2000).
  - <sup>29</sup>F. Cleri, S. R. Phillpot, D. Wolf, and S. Yip, *J. Am. Ceram. Soc.* **81**, 501 (1998).
  - <sup>30</sup>F. Cleri, S. R. Phillpot, and D. Wolf, *Interface Sci.* **7**, 45 (1999).
  - <sup>31</sup>V. Shastri and D. Farkas, *Modell. Simul. Mater. Sci. Eng.* **4**, 473 (1996).
  - <sup>32</sup>D. Farkas, *Philos. Mag. Lett.* **80**, 229 (2000).
  - <sup>33</sup>J. D. Eshelby, in *Dislocations in Solids*, edited by F. R. N. Nabarro (North-Holland, Amsterdam, 1979), Vol. 1, p. 169.
  - <sup>34</sup>A. Gerasoulis, *Comput. Math. Appl.* **8**, 15 (1982).
  - <sup>35</sup>K. K. Lo, *Trans. ASME, J. Appl. Mech.* **45**, 797 (1978).
  - <sup>36</sup>M. Y. He and J. W. Hutchinson, *Trans. ASME, J. Appl. Mech.* **56**, 270 (1989).
  - <sup>37</sup>J. Niu and M. S. Wu, *Eng. Fract. Mech.* **57**, 665 (1997).
  - <sup>38</sup>R. de Wit, *J. Phys. C* **5**, 529 (1972).
  - <sup>39</sup>A. P. Sutton and V. Vitek, *Philos. Trans. R. Soc. London, Ser. A* **309**, 1 (1983).
  - <sup>40</sup>A. P. Sutton and R. W. Balluffi, *Interfaces in Crystalline Materials* (Clarendon Press, Oxford, 1995).
  - <sup>41</sup>G.-J. Wang and V. Vitek, *Acta Metall.* **34**, 951 (1986).
  - <sup>42</sup>D. V. Bachurin, R. T. Murzaev, and A. A. Nazarov, *Phys. Met. Metallogr.* **96**, 555 (2003).
  - <sup>43</sup>A. A. Nazarov, D. V. Bachurin, O. A. Shenderova, and D. W. Brenner, *Interface Sci.* **11**, 417 (2003).
  - <sup>44</sup>S. M. Foiles, M. I. Baskes, and M. S. Daw, *Phys. Rev. B* **33**, 7983 (1986).
  - <sup>45</sup>Information about XMD—Molecular Dynamics for Metals and Ceramics is available through the web page, <http://xmd.sourceforge.net/about.html>.
  - <sup>46</sup>M. P. Allen and D. J. Tildesley, *Computer Simulations of Liquids* (Clarendon Press, Oxford, 1987).
  - <sup>47</sup>V. Vitek and T. Egami, *Phys. Status Solidi B* **144**, 145 (1987).
  - <sup>48</sup>A. A. Nazarov, O. A. Shenderova, and D. W. Brenner, *Phys. Rev. B* **61**, 928 (2000).
  - <sup>49</sup>O. A. Shenderova, D. W. Brenner, A. A. Nazarov, A. E. Romanov, and L. H. Yang, *Phys. Rev. B* **57**, R3181 (1998).
  - <sup>50</sup>M. S. Wu, A. A. Nazarov, and K. Zhou, *Philos. Mag.* **84**, 785 (2004).